Geroliminis, Nikolas, Zheng, Nan, and Ampountolas, Konstantinos (2014)
A three-dimensional macroscopic fundamental diagram for mixed bi-modal
urban networks. Transportation Research Part C: Emerging Technologies,
42. pp. 168-181. ISSN 0968-090X

http://eprints.gla.ac.uk/92996

Deposited on: 15 April 2014

A three-dimensional macroscopic fundamental diagram for mixed bi-modal urban networks

Nikolas Geroliminis [a,*], Nan Zheng [a] and Konstantinos Ampountolas [a, b]

[a] *Urban Transport Systems Laboratory*, *École Polytechnique Fédérale de Lausanne, 1015 Lausanne, Switzerland*
[b] *School of Engineering, University of Glasgow, Glasgow G12 8LT, United Kingdom*

ABSTRACT

Recent research has studied the existence and the properties of a macroscopic fundamental diagram (MFD) for large urban networks. The MFD should not be universally expected as high scatter or hysteresis might appear for some type of networks, like heterogeneous networks or freeways. In this paper, we investigate if aggregated relationships can describe the performance of urban bi-modal networks with buses and cars sharing the same road infrastructure and identify how this performance is influenced by the interactions between modes and the effect of bus stops. Based on simulation data, we develop a three-dimensional vehicle MFD (3D-vMFD) relating the accumulation of cars and buses, and the total circulating vehicle flow in the network. This relation experiences low scatter and can be approximated by an exponential-family function. We also propose a parsimonious model to estimate a three-dimensional passenger MFD (3D-pMFD), which provides a different perspective of the flow characteristics in bi-modal networks, by considering that buses carry more passengers. We also show that a constant Bus-Car Unit (BCU) equivalent value cannot describe the influence of buses in the system as congestion develops. We then integrate a partitioning algorithm to cluster the network into a small number of regions with similar mode composition and level of congestion. Our results show that partitioning unveils important traffic properties of flow heterogeneity in the studied network. Interactions between buses and cars are different in the partitioned regions due to higher density of buses. Building on these results, various traffic management strategies in bi-modal multi-region urban networks can then be integrated, such as redistribution of urban space among different modes, perimeter signal control with preferential treatment of buses and bus priority.

Keywords: bi-modal traffic, macroscopic fundamental diagram, passengers, public transport, clustering

1   Introduction

Transportation systems in real cities are complex with many modes of transport sharing and competing for limited road infrastructure. While there is a vast literature of the dynamics and the modeling of congestion for vehicular traffic, the effect of service stops (like when a bus or taxi stops to board and alight passengers) in the overall performance of a large-scale urban system still remains a challenge. It is intuitive that the effect of these stops in the network capacity is almost negligible during light demand conditions, but nowadays city centers are experiencing high level of congestion and the frequency in time and space of these stops is significantly high. While one bus traditionally creates more congestion than a moving car, the additional delay per passenger carrying is smaller for large bus occupancies, making buses a more sustainable mode of transport compared to cars.

---
* Corresponding author. Tel: +41 21 69 32481; fax: +41 21 69 35060
  E-mail addresses: nikolas.geroliminis@epfl.ch (N. Geroliminis), nan.zheng@epfl.ch (N. Zheng), konstantinos.ampountolas@glasgow.ac.uk (K. Ampountolas)

To understand the physics of urban mobility, traffic dynamics of multimodal urban networks need to be analyzed under various network structures. As multiple modes compete for limited urban space, conflicts and interactions are developed resulting in congestion. Existing literature on multimodal traffic mainly focuses on the design and operation of special bus lanes (Site and Filippi (1998), Daganzo and Cassidy (2008), Li et al. (2010), Tirachini and Hensher (2011)) or optimization of traffic signals with transit priority (Mesbah and Currie (2011), Christofa et al. (2013)). However there is no significant body of work dedicated on the modeling of traffic dynamics and the influence of each mode on the network performance. Most of the existing works fall short either in the scale of application or the treatment of congestion dynamics (small scale and/or static models). For example, the work by Li et al. (2010) estimates traffic state for each mode based on a BPR (Bureau of Public Roads, 1964) type of model, which works only for static conditions. Site and Filippi (1998), Daganzo and Cassidy (2010) and Tuerprasert and Aswakul (2010) utilize the link-scale Fundamental Diagram, which can experience high scatter and therefore cannot provide accurate estimates of speed and travel time at the network level. These somehow detailed models can also be computationally complex when applied at the network scale.

An aggregated modeling for multimodal systems, following the concept of a macroscopic fundamental diagram (MFD), can be a strong alternative if it unveils similar properties as in the single-mode case of vehicular traffic. The idea of an MFD for car-only urban networks was initially proposed by Godfrey (1969) and was re-initiated later in Mahmassani et al. (1987) and Daganzo (2007). The demonstration of its existence with dynamic features and empirical data from Yokohama was recent by Geroliminis and Daganzo (2008). This work showed that the MFD is a property of the network itself (infrastructure and control) if the network is homogeneously congested and not very sensitive to demand, i.e. the space-mean flow is maximum for the same value of critical density of vehicles, for many origin-destination tables. Recent works also highlighted that the spatial distribution of congestion can affect the shape and the scatter of the MFD with higher flows observed for less spatial heterogeneity, e.g. Mazoumian et al. (2010), Geroliminis and Sun (2011), Mahmassani et al. (2013), and Knoop et al. (2013). Analytical theories have been derived for the shape of the MFD as a function of network and intersection parameters, using variational theory for homogeneous and heterogeneous network topologies, respectively (Daganzo and Geroliminis (2008), Geroliminis and Boyaci (2012), Leclercq and Geroliminis (2013)). The properties of a well-defined MFD, stability and scatter phenomenon are analyzed through many other simulation studies and experimental tests, such as Buisson and Ladier (2009), Ji et al. (2010), Gayah and Daganzo (2011), Saberi and Mahmassani (2012), and Ji and Geroliminis (2012), Mahmassani et al. (2013). Given the MFD of a network, effective traffic management strategies can be readily developed to mitigate congestion, examples including perimeter flow control in Keyvan-Ekbatani et al. (2012), Haddad et al. (2012) and Aboudolas and Geroliminis (2013) and cordon-based pricing in Zheng et al. (2012). Besides, Gonzales and Daganzo (2012) examined system optimum solutions for a transport system with cars and public transit share spaces for the morning commute problem. The authors solved user and system optimum for the bottleneck model and system optimum for the network model (with an MFD representation).

Building on the knowledge of the single-mode MFD, developing and understanding the dynamics of multimodal networks is promising. In this work, we seek to extend the modeling and the application of the single-mode MFD to a bi-modal (bus and cars) one, with the consideration of passenger flows and traffic performance of each mode. If this type of models holds for further scrutiny in multimodal networks, then network level control strategies can be developed to maximize urban mobility. The dynamics of traffic flow in bi-modal networks are more complicated due to the operational characteristics of buses and the interactions between cars and buses. Despite of this complication, simulation studies on small networks showed that a classical MFD applies (under certain conditions) for bi-modal urban networks as well, see e.g. Gonzales et al. (2011) Zheng and Geroliminis (2013). However, the influence of each mode in the network dynamics and performance is still missing. This relationship, if known, will facilitate the development of control strategies at various levels, e.g. network bus priority (Christofa et al. 2013) or redistribution of urban space (Zheng and Geroliminis, 2013). Therefore we aim at investigating the relationship among the accumulation of cars and buses, and the traffic throughput or circulating flow of a network. Buses have scheduled service stops in addition to stops caused by traffic and signals, which makes the speed and the flow rate of buses lower than cars. On the other hand, buses carry significantly higher number of passengers. Therefore it is insufficient to simply consider vehicle flows and develop the relevant management strategies for a multimodal network. Zheng et al. (2013) presented initial simulation findings on a three-dimensional macroscopic relation between flow and accumulations for a bi-modal network, and proposed to develop a macroscopic passenger flow model.

A semi-analytical approach building on variational theory was developed to estimate an MFD for networks with cars and buses (Boyaci and Geroliminis, 2011). Buses influence traffic when they stop for passengers to enter or exit at bus stops. These stops were treated as periodic red phases of fictitious traffic signals that decrease the capacity of the road at the bus stop locations. While such a framework can provide important insights for network capacity for different operational characteristics of buses, it cannot directly integrate the heterogeneity in the spatial distribution of buses and cars in the network. To shed some light towards this direction a detailed micro-simulation of a congested bi-modal network is performed for various demand scenarios and a relationship between network flow and accumulations of cars and buses is investigated in the current work.

Both the vehicle flow and the passenger flow dynamics were not studied in detail and have to be further investigated. Furthermore, the ratio of car and bus density is not homogeneously distributed in urban networks (due to different location of bus lanes and service frequencies) and it is insufficient to assume a homogeneous interaction between the two modes for whole network. Thus, multimodal networks with significant presence of buses might experience different aggregated dynamics than car-only networks and might not follow an aggregated law similar to the MFD. In this case, network partitioning algorithms, such as the one presented in Ji and Geroliminis (2012) for car-only networks, can be applied to capture the spatial heterogeneity in flow characteristics.

The remaining part of the paper is organized as follows: Section 2 investigates the existence and the properties of a three-dimensional vehicular MFD (3D-vMFD) relating the accumulation of cars and buses, and the total circulating vehicle flow in the network based on simulation data with mixed traffic of cars and buses. Then a three-dimensional passenger MFD (3D-pMFD) is derived relating the accumulation of cars and buses and the passenger flow in a bi-modal network. Section 3 introduces an analytical approach to approximate the shape of the bi-modal passenger MFD, given the 3D-vMFD. Afterwards, we investigate how partitioning can contribute to the modeling of heterogeneous networks. The last section summarizes the findings and discusses future research directions.

2   A city-scale three-dimensional MFD for bi-modal traffic

In this section, we investigate the relation among accumulation of cars and buses and circulating flow (both vehicle and passenger) in bi-modal traffic networks via simulation experiments. We show that an area of Downtown San Francisco exhibits a city-scale three-dimensional vehicle MFD (3D-vMFD) relating the accumulation of cars and buses to flow with moderate scatter under different bi-modal demand patterns. We further show that our test site exhibits a city-scale three-dimensional passenger MFD (3D-pMFD) relating accumulation of cars and buses, to the passenger flows in the bi-modal network.

The test site is a 3 km^2 area of Downtown San Francisco including about 100 intersections and 430 links of total 100 lane-kms. The number of lanes varies from 2 to 5 lanes and the free flow speed is around 45 km/h. Traffic signals are all multiphase fixed-time operating on a common cycle length of 100 s for the west boundary of the area and 60 s for the rest. There is no any preferential treatment of buses, e.g. transit signal priority (TSP). Bus stops are in-lane of traffic and create queues of cars during stopping The traffic flow in the (bi-modal) network comprises two vehicle classes, i.e., passenger cars and buses. Bus routes and frequencies for lines in the studied network have been obtained from the San Francisco Municipal Transportation Agency (SFMTA). Bus stops are influencing traffic as in most cases there are on-street with a capacity for one or two buses to serve passengers. Cars and buses are sharing the same infrastructure and operating in the same road lanes except in Section 2.5, where a preliminary investigation of dedicated bus lanes is carried out.

2.1   A three-dimensional MFD for vehicle flows (3D-vMFD)

Let us denote by n_c the accumulation of cars and n_b the accumulation of buses at a specific time interval, Q_m is the total network circulating flow for each mode respectively, $m\epsilon\{b,c\}$ and Q the total network flow (in vehicle per unit time), which is the sum of car and bus circulating flows, all estimated during the same interval. Q_m is defined in accordance to Edie's definitions as $Q_m = \sum_i l_i q_{im}/L$, where l_i is the length of link i, q_{im} is the flow of link i at interval t for mode m and L is the average link length (Edie, 1963). For the developed model, the flow Q in the bi-modal network is considered to be a function of n_c and n_b given by (time interval t is omitted from the equations for simplicity)

$$Q = Q(n_c, n_b) = Q_c(n_c, n_b) + Q_b(n_c, n_b). \qquad (1)$$

1   To obtain the shape of (1) we perform extensive simulation experiments in the test network with
2   time-dependent asymmetric origin-destination tables, and different compositions of the bi-modal traffic (pairs
3   of n_c and n_b). The demand profile for cars is a typical peak-hour demand with a trapezoidal shape. For buses,
4   the demand is determined by the number of lines and their operational frequency using data from SFMTA.
5   Higher demand scenarios are also analyzed to generate various mode compositions. For the simulation
6   experiments, the test network is modeled via the AIMSUN microscopic simulator. The simulation horizon for
7   each experiment is 5.5 h and pairs of data (n_c, n_b) are gathered every 5 min from the simulator. For each
8   5-min interval, Q_b, Q_c are estimated as described above. Note that more than 20 scenarios with different
9   dynamic demand characteristics are carried out to generate the corresponding traffic performance Q for a wide
10 range of n_c and n_b. In the simulation, the dwell time was time-dependent with three different periods: the
11 onset of the peak-hour, peak-hour and the offset of peak hour. For each time period, the average dwell time
12 was fixed for all bus lines. However, the dwell times followed normal distribution, with a standard deviation
13 around 20% of the mean. This means that in some cases of low demand, the buses could skip one stop. Some
14 scenarios are analyzed later in more details.

15 Fig. 1(a) illustrates the 3D-vMFD for bi-modal traffic, $Q(n_c, n_b)$. As a first remark, Fig. 1(a) confirms the
16 existence of a 3D-vMFD for bi-modal networks, with a shape that depends on the accumulation of both cars
17 and buses. To enable a better understanding of this figure, Fig. 1(b) displays the contour plot of the 3D-MFD
18 on the (n_c, n_b) plane, using the Delaunay triangulation/interpolation algorithm (De Berg et al., 2008) to
19 estimate flow in a continuous space of the accumulation plane. The triangle in this figure indicates (n_c, n_b)
20 pairs, where the network operates close to the maximum throughput of the 3D-vMFD (values within the 80%
21 range of the maximum flow). In particular, it captures the "optimal operational regime" of bi-modal traffic.
22 City managers and practitioners could seek to derive management strategies to operate at this optimal regime.
23 It can be seen that the flow Q decreases monotonically as n_c and n_b increases, albeit with different slopes.
24 Remarkably, the slope of buses is higher that the slope of cars. This indicates that effect of an additional bus
25 in the network is much different than an additional car. A simple explanation is that buses make additional to
26 traffic signal stops for passengers, and negatively influence traffic by creating stop-and-go phenomena. The
27 figure also depicts critical accumulations of cars $\tilde{n}_c$ (rising line in the triangle) where Q reaches its maximum
28 for different values of n_b. The slope of the rising dashed line reflects that the capacity to serve cars has to be
29 compromised in order to serve more buses, approximately $\tilde{n}_c \cong 3500 - 0.5n_b$. As a general remark, the
30 3D-vMFD can be used by policy makers to exploit the trade-off between the operation of buses and cars and
31 design more sustainable cities. Note also that the maximum value of the network flow occurs for $n_b = 0$ and
32 $n_c = 3500$ because of the effect of bus stops. If one ignores the higher passenger bus occupancy, an optimal
33 strategy to maximize vehicle flow is to operate at the (3500,0) pair. The shape of the 3D-vMFD and the
34 "optimal operational regime" depends in the geometry of the network, the signal settings and the public
35 transport characteristics (location of stops, size and location of births, existence or not of transit signal priority
36 etc.). As we show in the next section, a consideration of different vehicle occupancies for buses and cars in the
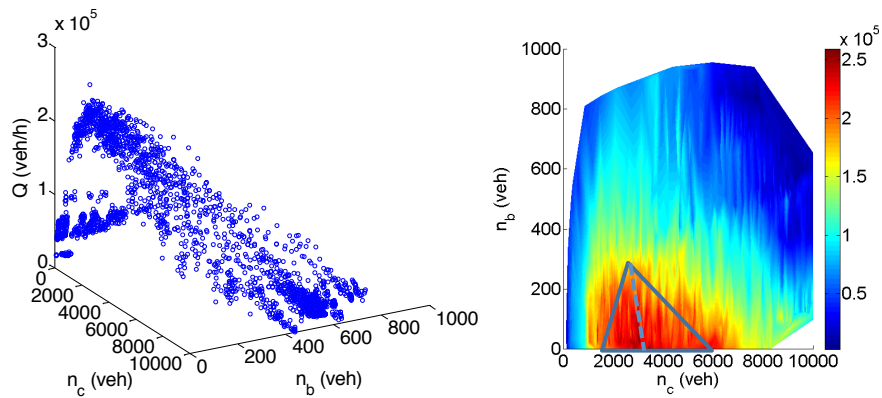37 estimation of network passenger flow will produce a different result.

38

39 Fig. 1. (a) The 3D-vMFD points for bi-modal traffic; (b) Contour plot of the 3D-vMFD after interpolation
40   by Delaunay triangulation. The color represents the value of circulating flow Q (vehs/h).

1   *2.2   A three-dimensional MFD for passenger flows (3D-pMFD)*

2 Given the 3D-vMFD in Fig. 1, incoming flow can be controlled at the boundary of the network in order to
3 operate at its "optimal operational regime". Existing methodologies for car-only perimeter control can be
4 found in Keyvan-Ekbatani et al. (2012), Haddad et al. (2012), Haddad and Geroliminis (2012), Aboudolas and
5 Geroliminis (2013) and elsewhere. However, these types of strategies are not able to consider that buses are
6 more efficient modes due to higher passenger occupancy and they might restrict bus flow from entering the
7 network. Before developing traffic management strategies for bi-modal systems with preferential treatment of
8 buses, dynamics of passenger flows have to be investigated.

9 Denote P the passenger flow in the bi-modal network, with n_c and n_b. We are interested in observing $P =$
10 $P(n_c, n_b)$. Denote h_m the average number of on-board passenger occupancy per vehicle, $m\epsilon\{b,c\}$. We
11 assume that car occupancy h_c is constant $h_c = 1.3$, while we estimate bus occupancy h_b as an increasing
12 function of the dwell times (similar to Zheng and Geroliminis, 2013). Dwell times are time-dependent, with
13 three periods: on-set, during and off-set of peak hour. Dwell times are stochastic following a bounded normal
14 distribution, so to capture some uncertainty in passenger demand (in the simulation, only dwell times are
15 available). Then, by definition, total passenger flow P can be expressed as

$$P(n_c, n_b) = h_c Q_c(n_c, n_b) + h_b Q_b(n_c, n_b) \tag{2}$$

16 We estimate passenger flows via the available simulated data, with the measurements of car flows Q_c, bus
17 flows Q_b and the estimated bus occupancy h_b (direct simulation of passenger movements is not possible in the
18 simulation). We use the same simulated flow data as the ones used to construct Fig. 1(a). Fig. 2(a) illustrates
19 the 3D-pMFD relating accumulation of cars and buses to passenger flows. This figure presents a 3D-MFD
20 like-shape for passenger flow, which looks similar with Fig. 1(a), but with higher maximum value, due to the
21 h_b term in equation (2). Nevertheless, a more careful look through the contour plot reveals significant
22 differences.

23 Fig. 2(b) depicts the resulting contour plot of P on the (n_c, n_b) plane after applying the same triangulation
24 algorithm as in Fig. 1(b). The polygon in this plot captures the "optimal operational regime" of passenger flow
25 of bi-modal traffic. It can be seen that the shape of the region is significantly different from the one observed
26 in Fig. 1(b). More precisely, for a given n_c passenger flow P first monotonically increases as n_b increases to a
27 critical $\tilde{n}_b$ and then decreases for $n_b > \tilde{n}_b$. Thus, having buses in the network will significantly increase the
28 efficiency of the system but overloading the network with buses will eventually cause delays for all vehicles
29 and reduce passenger throughput. The figure also displays that $\tilde{n}_c$ in this case (rising dotted line in the
30 polygon) has a clear tendency of becoming smaller as n_b increases, $\tilde{n}_c \cong 3500 - 6n_b$. The slope of the rising
31 line reflects that only a slight increase of buses can allow a large reduction of cars to maintain the same
32 passenger flow, which was not the case in the $Q(n_c, n_b)$ plot. The maximum network flow occurs now for a
33 positive n_b, the pair (2800, 120). It can be foreseen that more buses can be deployed in the network to succeed
34 a higher passenger flow if dedicated bus lanes are provided. For example, Zheng and Geroliminis (2013) tried
35 to optimize passenger flows in a bi-modal network by redistributing the road infrastructure and offering a
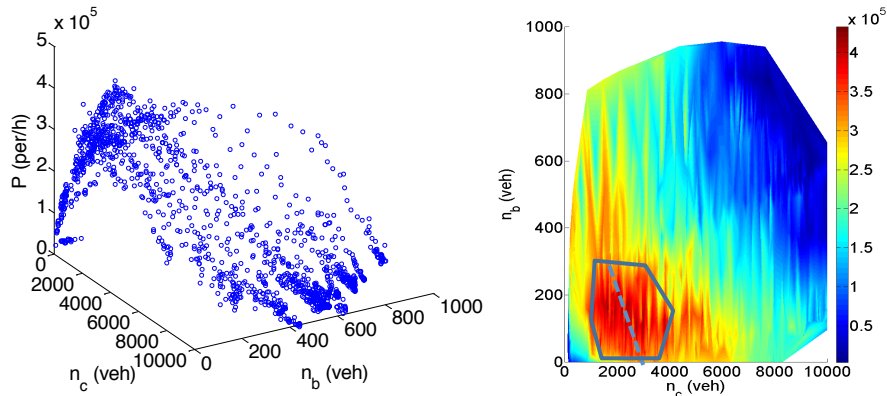36 fraction of roads for dedicated bus lanes.

38 Fig. 2. (a) The 3D-pMFD for bi-modal passenger traffic; (b) Contour plot of the 3D-pMFD,
39 the color represents the value of flow P (pers/h).

1   *2.3   A functional form of $Q(n_c, n_b)$ and $P(n_c, n_b)$*

2   Given that evaluating $Q(n_c, n_b)$ in (1) for many pairs of n_c and n_b is tedious, we propose instead using an
3   analytical function that approximates the 3D-vMFD in Fig. 1(a). Given the properties of $Q(n_c, n_b)$ described
4   in the previous section, we consider an exponential-family function, which has useful algebraic properties. In
5   general exponential families are in a sense very natural distributions to consider with plenty of applications in
6   physics and statistics. Note that parabolic families do not provide a good fit given their single value of the 2nd
7   derivative. To this end, we consider the following exponential flow function for data fitting:

$$Q(n_c, n_b) = a(n_c + n_b)e^{bn_c^2 + cn_b^2 + dn_c n_b + en_c + fn_b} \tag{3}$$

8   where a, b, c, d, e, f are model parameters. The parameter values should be specified so as to minimize the
9   deviation of model (1) from the corresponding measured values Q'. This function can be considered as a
10   generalization of the Drake's exponential function for a single-mode fundamental diagram between flow and
11   density. An unconstrained estimation will not be consistent with the physics of traffic, thus constraints (4b)
12   are added. To this end, we estimate the values by Least-Squares parameter estimation for the given simulated
13   data Q' in Fig. 1(b). The constrained parameter estimation problem is formulated as follows (P1):

$$\min_{a,b,c,d,e,f} Z = \|\boldsymbol{Q} - \boldsymbol{Q}'\|^2 \tag{4a}$$

subject to

$$\begin{cases} Q \geq 0, \quad \text{for} \quad 0 \leq n_c \leq \max(n_c) \text{ and } 0 \leq n_b \leq \max(n_b), \\ \dfrac{\partial V(n_c, n_b)}{\partial n_c} \leq 0, \quad \text{for} \quad 0 \leq n_b \leq \max(n_b), \\ \dfrac{\partial V(n_c, n_b)}{\partial n_b} \leq 0, \quad \text{for} \quad 0 \leq n_c \leq \max(n_c), \end{cases}$$

$$\tag{4b}$$

14   where V is the space-mean speed in the network, $\boldsymbol{Q}, \boldsymbol{Q}'$ are vectors with elements of the model (2) and the
15   simulated data for each 5 min sample interval, respectively. The space-mean speed is given by $V(n_c, n_b) \overset{\text{def}}{=}$
16    $QL/(n_c + n_b)$, where L is the average link length of the network. The first constraint in (4b) guarantees
17   non-negative flows for values of accumulation between zero and jammed. The second and the third constraint
18   emphasize that the space-mean speed of all vehicles should decrease monotonically as n_c and n_b increase.

19   The constrained parameter estimation problem (P1) is nonlinear and is solved through the Sequential
20   Quadratic Programming (SQP) approach. SQP method solves a sequence of optimization sub-problems, each
21   of which optimizes a quadratic model of the objective subject to a linear relaxation of the constraints. We
22   apply this algorithm for multiple initial values (around 1000) to avoid convergence to local minima, which
23   might be the case of non-smooth data. The estimated parameters resulting from the optimization problem are:
24    $\{a, b, c, d, e, f\} = \{1.95 \cdot 10^2, -2.34 \cdot 10^{-9}, 5.28 \cdot 10^{-7}, 6.34 \cdot 10^{-8}, -2.92 \cdot 10^{-4}, -1.50 \cdot 10^{-3}\}$. The T-test
25   result indicates that all six parameters are statistically significant (p-value almost zero). Fig. 3(a) illustrates
26   the results of fitting model (P1) with the estimated parameters to the simulated data. An R-square value of
27   0.91 (close to 1) indicates that the resulting 3D-vMFD fits well with the data and all physical constraints (4b)
28   are satisfied. We also verify the adequate fitting performance of the model by 3 different demand scenarios,
29   which were not used for model estimation and have different demand profiles. Fig. 3(b) depicts the contour
30   plot of the 3D surface on the (n_c, n_b) plane. Comparing Fig. 3(b) with Fig. 1(b), we can see that most patterns
31   observed closely matches each other except the area for very high values of buses $n_b > 600$ due to lack of
32   simulated data. Nevertheless, these states cannot be easily observed in real systems. Moreover, it can be seen
33   that the "optimal operational regime" (triangle in Fig. 1(b)) of bi-modal traffic is reproduced in a very similar
34   way.

35   We perform a similar optimization for fitting the measured passenger flow P with parameters
36    $a', b', c', d', e', f', g'$ for an exponential function $P(n_c, n_b) = a'(n_c + g'n_b)e^{b'n_c^2 + c'n_b^2 + d'n_c n_b + e'n_c + f'n_b}$.
37   Denote this parameter estimation problem as (P2). Solving (P2), we get $\{a', b', c', d', e', f', g'\} = \{3.46 \cdot$
38    $10^2, 6.41 \cdot 10^{-10}, -2.27 \cdot 10^{-6}, -1.14 \cdot 10^{-7}, -3.77 \cdot 10^{-4}, -5.30 \cdot 10^{-4}, 3.66 \cdot 10^0\}$. Fig 3(c) depicts the

result of the fitting model with the parameters. An R-test value of 0.91 (close to 1) indicates a decent model fitting, as well. Fig. 3(b) depicts the contour plot of the 3D surface on the (n_c, n_b) plane. Nevertheless, by comparing the parameters of the two models, no physical interpretations can be made. In section 3 we provide an analytical derivation to estimate $P(n_c, n_b)$ from $Q(n_c, n_b)$, without the need of curve-fitting, which unveil interesting properties of network traffic flows.
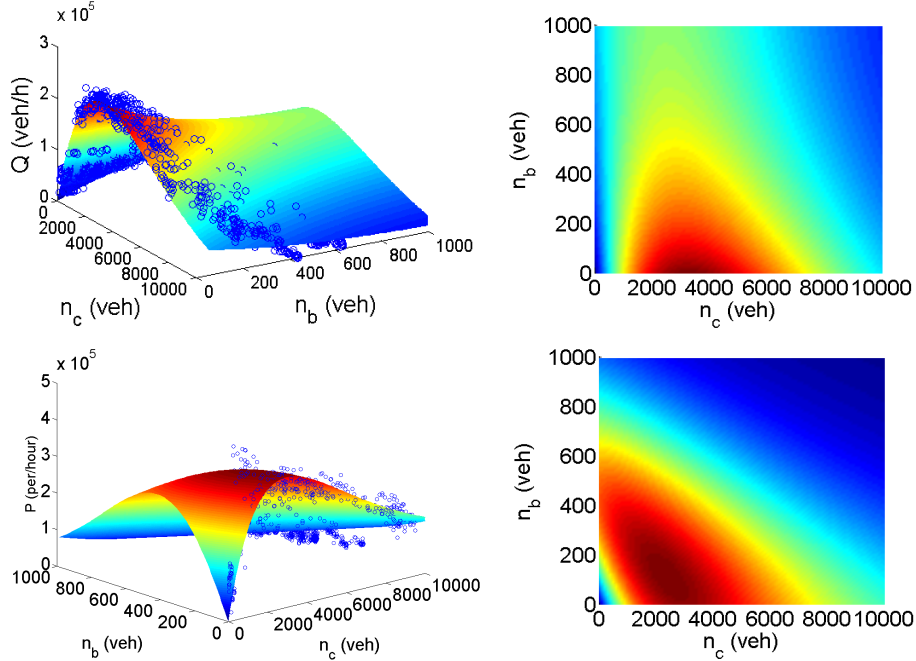

Fig. 3. (a) The exponential $Q(n_c, n_b)$; (b) Contour plot of $Q(n_c, n_b)$; (c) The exponential $P(n_c, n_b)$ and (d) Contour plot of $P(n_c, n_b)$.

2.4   Bus-Car Unit (BCU) equivalent

In transportation planning and analysis of bi-modal systems, it is a common approach to assume that each bus is equivalent to a constant number of cars independent of the level of congestion and the densities of each mode. This simplifies the derivations of different performance measures. Nevertheless, it is clear from the explanation of the previous section that the influence of buses in the network performance depends on the state of the system (n_c, n_b) and cannot be considered constant. Thus, a static BCU consideration is insufficient to reflect the dynamic relationship between bus/car accumulation and congestion. For this reason, we propose here an analytical estimation of the BCU value as a function of the accumulation of both modes.

Let us consider that the average network speed is $V(n_c, n_b) \stackrel{\text{def}}{=} Q(n_c, n_b) L / (n_b + n_c)$. We assume that for a given n_b, $V(n_c, n_b)$ is monotonically decreasing function of n_c and the same assumption for n_c (see the 2nd and 3rd constraint in equation 4b). Given that $V(n_c, n_b)$ is a continuous and differentiable function, we can estimate the effect that buses and cars have in speed V for a given (n_c, n_b) pair. Mathematically speaking, BCU is defined and estimated as the ratio of partial derivatives with respect to n_c and n_b

$$BCU(n_c, n_b) = \frac{\dfrac{\partial V(n_c, n_b)}{\partial n_b}}{\dfrac{\partial V(n_c, n_b)}{\partial n_c}} \tag{5a}$$

By assuming the closed form solution of $Q(n_c, n_b)$ in (3) and after some algebra we obtain

$$BCU(n_c, n_b) = \frac{2cn_b + dn_c + f}{dn_b + 2bn_c + e} \tag{5b}$$

Fig. 4 plots $BCU(n_c, n_b)$ which is a monotonically decreasing function of vehicle accumulations. Physically speaking, Fig. 4 highlights that the effect of buses in the network speed is smaller as the network is more congested. This is because dwell times at bus stops are a smaller fraction of car travel time compared to free-flow conditions. For example, in case of 10% bus accumulation, BCU values range between 5.0 for free-flow conditions to 3.5 for highly congested conditions.
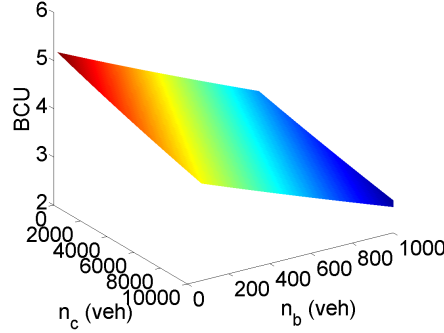

Fig. 4 A 3D diagram relating accumulation of cars and buses with BCU.

Nevertheless, equation (5a) might not be straightforward to estimate with real data without curve fitting, due to the scatter of the MFD measurements, that might make the estimation of derivatives complicated. An approximation of (5a) based on engineering principles, $BCU^*(n_c, n_b)$, can be obtained if we consider for a given pair of (n_c, n_b), an equivalent system with "cars only" that satisfies $V(n_{c0}, 0) = V(n_c, n_b)$, where n_{c0} is the accumulation of cars for a car-only network, i.e. $n_b = 0$. Thus, $BCU^*(n_c, n_b)$ is the solution of the equation $n_{c0} = n_c + BCU^* \cdot n_b$. In other words, BCU expresses an equivalent system with cars only that has the same space-mean speed with the mixed-traffic network. Then the average speed can be rewritten as

$$V(n_c + BCU^* \cdot n_b, 0) = V(n_c, n_b) \tag{6a}$$

Combining the functional form (3) and equation (6a), we obtain an analytical solution of BCU as a solution of the quadratic equation $bn_b BCU^{*2} + (2bn_c + e)BCU^* - cn_b - dn_c - f = 0$, which is given by

$$BCU^*(n_c, n_b) = \frac{-(2bn_c + e) - \sqrt{(2bn_c + e)^2 + 4bn_b(cn_b + dn_c + f)}}{2bn_b} \tag{6b}$$

Given that the value of b is relatively small, BCU estimation can be approximated (error less than 0.01 by the solution of $eBCU - cn_b - dn_c - f = 0$ and therefore gives the BCU^* a plane shape). These results also indicate that the BCU^* value for buses becomes smaller as congestion increases. While this result might be considered as counter-intuitive, it is consistent with the physics of traffic because the effect of bus related stops is a smaller part of the total travel time for congested conditions.

2.5   A macroscopic fundamental diagram for buses operating in dedicated lanes

As dedicated bus lane allocation is a sustainable strategy for multimodal urban transportation systems with preferential treatment of higher occupancy modes of transport, it deserves the effort to look into a city-wide MFD for buses running in dedicated bus lanes. While a detailed analysis is beyond the scope of this paper, we perform an analysis where all the bus lines perform in dedicated lanes. To this end, the existing test site is updated and one lane in each road of the city center with public transport lines is assigned to buses if space is available. The resulted bus-lane network is well connected and includes about 5 km of dedicated bus lanes. To

derive and investigate the shape of the MFD for buses, simulations are performed with a field-applied fixed-time plan and a fixed number of bus lines. To account for demand effects of the bi-modal traffic composition, ten runs were carried out for a 4-h time-dependent scenario with different car demand and bus frequency. Additionally, two scenarios (with five runs each) based on different dwell time of buses were defined in order to investigate the impact of the dwell time in the shape of the MFD for buses. Fig. 5 displays the MFD for buses resulting for the aforementioned runs. This figure plots the network flow-density relationship (buses/5min vs. buses/km) in the network for the whole simulation time period. Each measurement point in the diagram corresponds to 5 min interval. Fig. 5(a) confirms the existence of an MFD for buses with moderate scatter across different scenarios. Note that the value of critical density and maximum flow are considerably smaller compared to the ones of the vehicle MFD (critical density around 7 buses/km and capacity around 70 buses/hr).

It can be seen that the free flow speed in the bus lanes is around 25 km/h and the maximum flow occurs in a density range from 5 to 10 buses per km. If the density is allowed to increase, then the dedicated bus lanes become severely congested. The flow decreases with density (negative slope) and the network can lead to gridlock. This MFD like-shape for buses operating in dedicated lanes is quite conforming to the MFD for cars and mixed traffic. An interesting observation is that the diagram indicates a high flow scatter for the critical bus density $\hat{k}_b$. This difference is attributed to different traffic patterns for the cars and the interaction of the bi-modal traffic at the intersections that could lead to partially block of the dedicated bus lanes due to spillbacks. Besides bus frequency, the effect of the dwell times in the shape of the MFD is analyzed as longer dwell times reduce the average speed and flow. Fig. 5(b) illustrates the impact of different dwell time of buses on the MFD, plotting the MFD for buses resulting for multiple scenarios, where half scenarios have average dwell time of 25 s and the other 45 s. It can be seen that the higher dwell times lead to smaller flow capacity (in buses/hr), by about 15%. But, if we consider that bus occupancy might be almost double with higher dwell times, then the efficiency of the specific dedicated bus lanes in terms of passengers significantly increases. A higher number of bays to simultaneously serve buses at the same stop might also increase the network bus capacity. Optimal redistribution of road space between buses and cars, and the effect of such strategy in the mode choice are not described in this work. A theoretical approach towards this direction has been introduced in Zheng and Geroliminis (2013).
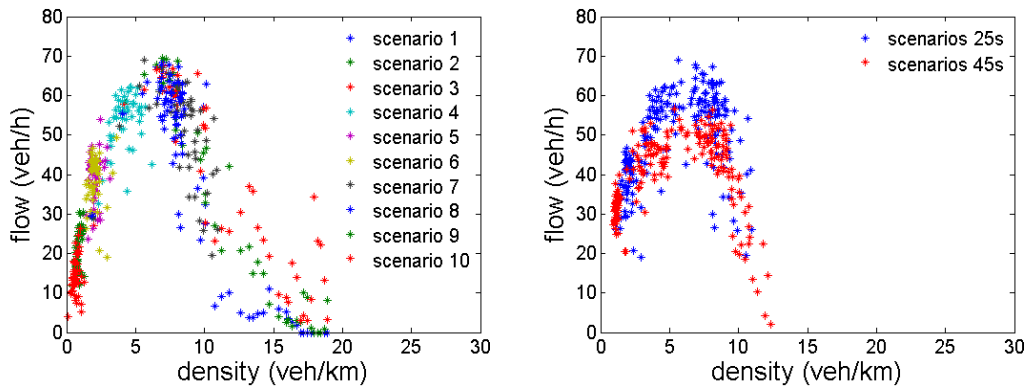

Fig. 5. (a) The MFD for buses for ten runs with different bi-modal traffic patterns; (b) The impact of different average dwell times of buses on the MFD.

3   An analytical model for the estimation of passenger flows

To maximize the passenger flow of a network and thus realize the efficiency of a multimodal network, we should seek a 3D-pMFD that can capture the dynamics of passenger flows but also can be derived from (3) rather than curve fitting. To this end, we describe a derivation of the analytical form of the passenger flow 3D-pMFD based on the vehicle flow 3D-vMFD in this section. We further show that by partitioning the network into regions with homogeneous traffic and mode composition, the analytical model is able to reproduce the passenger flow pattern as observed from the data.

1   *3.1   The derivation of a bi-modal MFD for passenger flow*

2   Let us investigate the analytical derivation of P given the analytical form of Q in (3). Our first objective is to
3   estimate flows Q_c and Q_b for each mode by utilizing Q, n_c and n_b. To this end, we first consider that
4   $V = (v_c n_c + v_b n_b)/(n_c + n_b)$ where v_c is the speed of car and v_b the speed of bus, and Q is given by

$$Q = Q_c + Q_b = (v_c n_c + v_b n_b)/L \qquad (7)$$

5   To estimate the individual flows of each mode, a relationship between their speeds is necessary, $v_b =$
6   $v_c(n_c, n_b)$. To obtain v_b as function of v_c, we utilize a first order approximation, a linear model between v_c
7   and v_b

$$v_b \cong \theta v_c + \beta, \qquad (8)$$

8   where θ and β are parameters that can be estimated with real data and depend on the operational
9   characteristics of the buses, the network topology and the composition of traffic in the network. Alternatively,
10 one can use a more detailed speed model, as for example the one proposed in Zheng and Geroliminis (2013),
11 where the average distance between successive bus stops and the average dwell time at a bus stop influence
12 the relation between v_b and v_c. We show later that model (8) can give a decent approximation of v_b.
13 Nevertheless, parameters θ and β might not be universal and depend on the ratio of buses and cars in the
14 network, n_c/n_b. The aforementioned models might be less accurate in case of bus bunching, where multiple
15 buses are queued in a bus stop with limited berths for boarding and alighting. A more detailed queuing model
16 can be derived in such a case. By introducing (8) in (7), we can obtain the analytical form of v_c. Then after
17 some algebra we estimate Q_c and Q_b as follows ($Q(n_c, n_b)$ is noted as Q):

$$Q_c = v_c n_c = \frac{QL - \beta n_b}{(n_c + \theta n_b)} \frac{n_c}{L} \qquad (9)$$

$$Q_b = v_b n_b = \left(\frac{QL - \beta n_b}{(n_c + \theta n_b)} \theta + \beta \right) \frac{n_b}{L} \qquad (10)$$

18 A physical interpretation of such equations is that as bus is a slower mode, the fraction of bus flow is smaller
19 than the fraction of bus accumulations. Then we derive $P(n_c, n_b)$ by combining (2), (9) and (10).

$$P(n_c, n_b) = h_c \left(\frac{Q(n_c, n_b)L - \beta n_b}{(n_c + \theta n_b)} \right) \frac{n_c}{L} + h_b \left(\frac{Q(n_c, n_b)L - \beta n_b}{(n_c + \theta n_b)} \theta + \beta \right) \frac{n_b}{L} \qquad (11)$$

20

21 Note that the 3D-*p*MFD is a function of the 3D-*v*MFD, the individual accumulations of buses and cars,
22 (n_c, n_b) and the average link length, L. A validation of the analytical model is provided later.

23

24 *3.2   Network partitioning*

25 By using a single value of θ and β in (8) for the whole network, one assumes that the interaction between cars
26 and buses is homogeneous in space and time. Nevertheless, the analytical estimation in (11) cannot accurately
27 reproduce $P(n_c, n_b)$, if $Q(n_c, n_b)$ is assumed to follow the exponential model (3). The reason is simple, bus
28 lines are not evenly distributed in the studied network. The ratio δ_i between the density of bus k_{bi} and density
29 of cars k_{ci} (where i is a link) is much higher in the center of the network, where there is higher frequency and
30 density of bus lines. Fig. 6(a) displays the bus routes of the simulated network, which match the real ones.
31 Note that some lines share links with the others in the center part of the network and that not all the lines can
32 be visualized in the figure. We can observe that, the center area of the network ($x\epsilon$ [2500, 4000], $y\epsilon$ [3500
33 4500]) includes more bus lines than the other parts of the network. Let us take δ_i at a certain time interval
34 during the simulation, when the network is operating at its maximum flow rate. Fig. 6(b) illustrates the scale
35 distribution of δ_i by a grey-scale plot, where a darker color indicates a higher value of δ_i. This result shows

1   that there exists a strong heterogeneity in the spatial distribution of δ_i, especially when comparing the mode
2   composition between the center area (roughly identified) and the rest of the network. Note also that the same
3   part of the network with higher δ_i, experiences more congestion than the remaining part.

4   To this end, we partition this network for the sake of homogeneity of δ_i within each partitioned regions. This
5   partitioning builds in a clustering algorithm proposed in Ji and Geroliminis (2012) for heterogeneously
6   congested networks. The objectives of partitioning are to obtain (i) small variance of link ratio δ_i within a
7   cluster and (ii) spatial compactness of each cluster, which makes feasible the application of perimeter control
8   strategies. The partitioning mechanism consists of three consecutive algorithms. Firstly, an over segmenting
9   of the network is provided by a sophisticated algorithm (Shi and Malik, 2000). Secondly, a merging algorithm
10 is developed based on initial segmenting and a rough partitioning of the network is obtained. Finally, a
11 boundary adjustment algorithm is designed to further improve the quality of partitioning by decreasing the
12 variance of δ_i while keeping the spatial compactness of the clusters. The similarity between links i and
13 $j, w(i,j),$ is given by

$$w(i,j) = \begin{cases} \exp\left(-\left(\delta_i - \delta_j\right)^2\right), & if\ r(i,j) = 1 \\ 0, & o.w. \end{cases} \tag{12}$$

14 where $r(i,j)$ is the spatial distance between two links denoted by the length of the shortest part between i and
15 j. Equation (12) simply explains that if two links are not adjacent, their similarity is negligible. Such an
16 approach, can guarantee that the developed clusters will be well-connected (compact) and the topological
17 characteristics influence links in the same cluster. For a detailed description, the reader should refer to Ji and
18 Geroliminis (2012). The studied network is divided into two regions (clusters) as shown in Fig. 6(c) after the
19 application of the algorithm. Let us denote these two regions the "center region" and the "outside region"
20 respectively, where the center region has more bus lines. We can see that this result closely matches what we
21 have observed from the data in Fig. 6(b). Note that, the partition algorithm by its nature tries to give a
22 compact shape with smooth boundaries of the partitioned regions. This explains why the exact shape of the
23 area with high value of δ_i is not fully obtained. The objective of partitioning is satisfied as the mean value of
24 δ_i in the center region is much larger than the one in the outside region, $(\delta_{center}, \delta_{outside}) = (0.40, 0.04)$.
25 The mean value of δ_i in the whole network is 0.20 (around 16% of vehicles are buses). The standard deviation
26 of δ_i is 0.45 for the center region and 0.12 for the outside region, which is smaller compared to 0.76 for the
27 whole network. This means that the algorithm succeeds to cluster together links with more similar δ_i. Note
28 that standard deviations are high because in both sub-regions there are plenty of links with no buses, $\delta_i = 0$
29 and in the center region there are some links with bus bunching (and high δ_i).

30 We are interested in investigating if this partition reduces the heterogeneity of congestion as well. Therefore,
31 we calculate the total density k_i ($k_i = k_{ci} + k_{bi}$) of link i in each partitioned region and comparing the
32 variance of k_i within each region, when the network vehicle flow is maximum. The mean values of k_i are 15
33 veh/km for the whole network, while 18veh/km for the center region and 13 veh/km for the outside region.
34 The standard deviation of k_i is 9 veh/km for the center region and 6 veh/km for the outside region, which is
35 again smaller compared to a value of 16 veh/km for the whole network. It shows that a
36 mode-composition-based partitioning is sufficient to reduce heterogeneity of 3D-MFD. In reality this may not
37 always be the case, if the scale of flow densities is not similar among links. In those cases, one may apply a
38 partition algorithm based on both δ_i and k_i, e.g. using a different similarity function in (12). As we show in
39 the next section, the resulting partitioning is sufficient for understanding the traffic heterogeneity and provides
40 a good approximation of the 3D-pMFD.

41 Furthermore, we verify the usefulness of the partitioning from a traffic point of view, by examining the time
42 when each region reaches congestion. Here, "congestion" starts when network flow drops after the network
43 reaches its maximum flow. To compare regions of different sizes, instead of accumulations we utilize
44 densities. Fig. 7(a) shows the MFD (vehicle flow $Q = Q_b + Q_c$ vs. vehicle density $k = \sum_i k_i$) of the center
45 region, the outside region and the whole network respectively, for one scenario. Density of buses and cars
46 (k_b, k_c) are estimated by dividing accumulations with the total lane kilometers utilized by each mode,
47 $L_b^{center} = 24$ ln-km, $L_c^{center} = 37$ ln-km, $L_b^{outside} = 26$ ln-km, $L_c^{outside} = 64$ ln-km, $\{b, c\}$ for bus and car
48 respectively. The start of congestion in each region is indicated by an arrow with the corresponding timestamp

11

attached. We can observe that the center region reaches congestion first, half hour earlier than the outside region. Fig. 7(b) displays the time series of the average density of the two regions respectively. Note also, that density in the center region is consistently higher than in the outer region between 9:30 and 12:00. Thus, a static partitioning (based on the conditions at 10am) succeeds to identify the more congested region of the network. This conclusion should not be universal as in case of different demand profiles and congestion propagation in time and space, partitioning should be re-evaluated in a dynamic way. The direction of dynamic partitioning is a challenging future area of research. The fact that regions of a network have various levels of congestion is important, as it indicates that different traffic management measures should be applied for the two regions based on their individual traffic states.
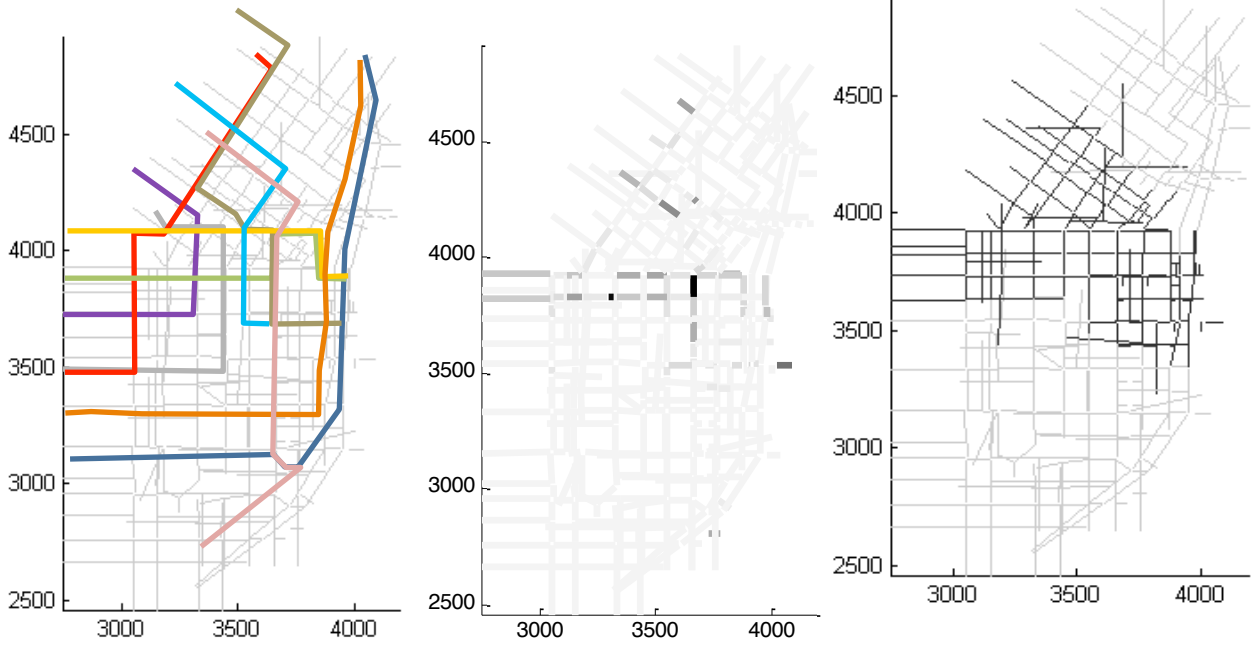

Fig. 6. Illustration of the partitioned network: (a) Layout of the bus lines over the network; (b) Contour plot of link ratio δ_i; and (c) Result of partitioning.
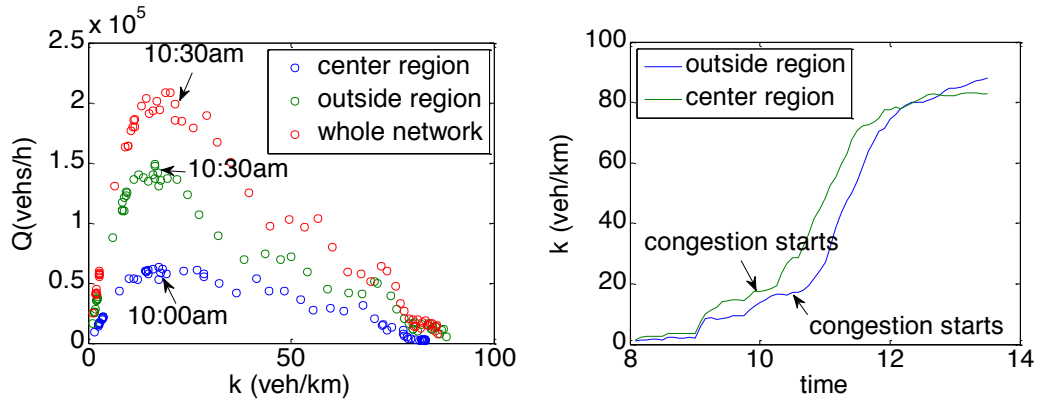

Fig. 7 Comparing the time each region reaches congestion in (a) Network flow-density relation and (b) Density time-series.

3.3 *Vehicle 3D-vMFD after partitioning*

Let us now show the 3D-*v*MFD for the partitioned regions. We utilize the data of the same scenarios as in Fig. 1. To have the scale of the MFDs of the two regions comparable, we normalize the values of accumulations and reproduce densities. Denote density of cars k_c and density of buses k_b, as estimated in the previous section. Given that the one region is larger than the other, we also normalize network flows by the maximum value of flow observed in each region. The normalized 3D-*v*MFDs for the two partitioned regions are plotted

in Fig. 8(a). k_b of the center region has a higher range of values, as the region is covered by more bus lines. Nevertheless, the general pattern observable in Fig. 8(b) and (c) is similar to the 3D-vMFD as observed in Fig. 3, especially the values of critical densities (for example 35vh/km * 100 ln-km =3500 veh which is the critical accumulation of Fig. 3b). Given the 3D-vMFD of each region, specific management measures such as perimeter signal control can be applied with the objective of operating at the region's optimal regime.
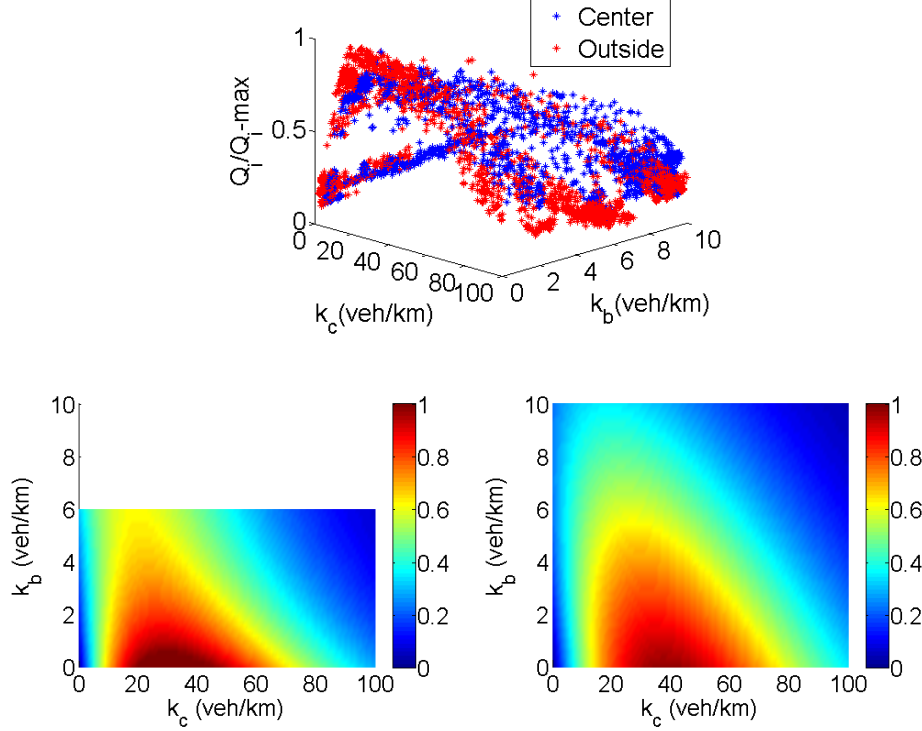

Fig. 8 (a) The normalized 3D-MFD of the partitioned regions; the contour plots on (k_c, k_b) plane for (b) The center region and (c) The outside region.

3.4 *Passenger 3D-pMFD after partitioning*

Let us compare the resulting passenger dynamics of one scenario before and after partitioning. Both vehicle and the passenger MFDs are displayed in Fig. 9(a) for the whole network. Given that ratio δ is not significantly varying with time during the specific scenario, passenger flow $P(n)$ vs. total accumulation $n = n_b + n_c$ is displayed. Even without partitioning the network has a low scatter MFD with a well-defined maximum flow and a clear value of critical accumulation (Fig. 9a). The vehicular flow MFD, $Q(n)$, has a similar shape, but the value of critical accumulation is larger.

Let us have a more careful look in the results after partitioning. Fig. 9(b) plots n_b vs. n_c with time for the two partitioned regions. It can be seen that the center region has a δ of about 9%, which is 6 times larger than δ in the outside region, where δ is the ratio $\sum_i n_{bi} / \sum_i n_{ci}$, i is the link. Fig. 9(c) depicts the space-mean speed for each region and mode. The dashed lines indicate the fitting results of equation (8). Parameter θ for the center region is 0.3 and for the outside region is 0.5, while β is 0 in both cases. The resulting linear relationship is consistent with the proposed approximation in (8). If equations (8) to (11) were applied to estimate $P(n)$ for the whole network, errors would not be negligible because of differences in δ and θ between the two regions. Fig. 9d shows the estimated $P(n_c, n_b)$ for the center and outside region after applying (8) – (10).

Let's now consider the performance of (8) – (11) for the partitioned regions for three different scenarios with various bus demands, denoted as "s₁", "s₂" and "s₃". After applying the partitioning algorithm, δ and θ are estimated for the center and outside region and passenger MFDs are plotted. Note that partitioning is static and is not re-estimated for different demand scenarios, because similar performance with respect to homogeneity metrics is achieved with Section 3.2. Nevertheless, dynamic partitioning algorithms are expected

to improve the homogeneity of congestion distribution, especially for networks with propagation in both time and space and multiple pockets of congestion.
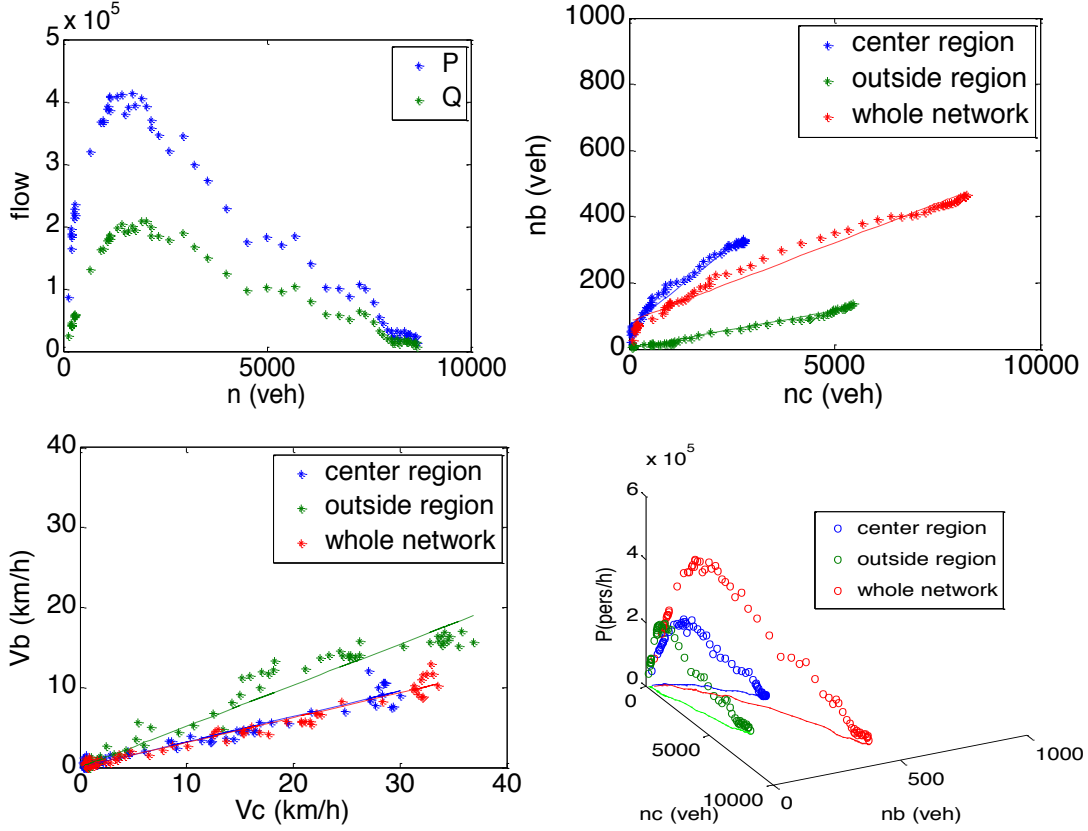

Fig. 9 (a) Passenger MFD from the simulation; (b) n_b vs. n_c; (c) v_b vs. v_c; and (d) The estimated passenger MFD for the two partitioned regions and the whole network.

The total network passenger flow is estimated as

$$P(n_c(t), n_b(t)) = P_1(n_{c1}(t), n_{b1}(t)) + P_2(n_{c2}(t), n_{b2}(t)) \tag{13}$$

where indices 1 and 2 represent the two partitioned regions, center and outside. Fig. 10(a) shows accumulation of buses and cars for the entire network for the three scenarios. The red dotted line ("s₃") represents the same scenario as of Fig. 9. The orange circles highlight the accumulation pairs where maximum flow is achieved in each scenario. Note the different values of mode composition δ for each scenario. Fig. 10(b) depicts the corresponding $P(n_c, n_b)$ of the three different scenarios, and the δ of each scenario is projected on the (n_c, n_b) plane. We can see that, by applying the estimated θ based on partitioning, the analytical model is able to reproduce the important patterns as observed in Fig. 2(b): (i) P increases and then decreases as n_b increases, (ii) the critical accumulation largely shifts towards the left, and (iii) there exists an "optimal operational regime" where the same value of maximum P (close to critical value) can be achieved with different combinations of n_b and n_c. Fig. 10(c) compares the estimated P from the model with the measured P from the simulation for the whole network, clearly showing that with partitioning P can be obtained more accurately. Furthermore by comparing the estimated passenger flow with and without partitioning, we find that the mean absolute error has a 10% improvement (the higher the value of δ, the higher the improvement).
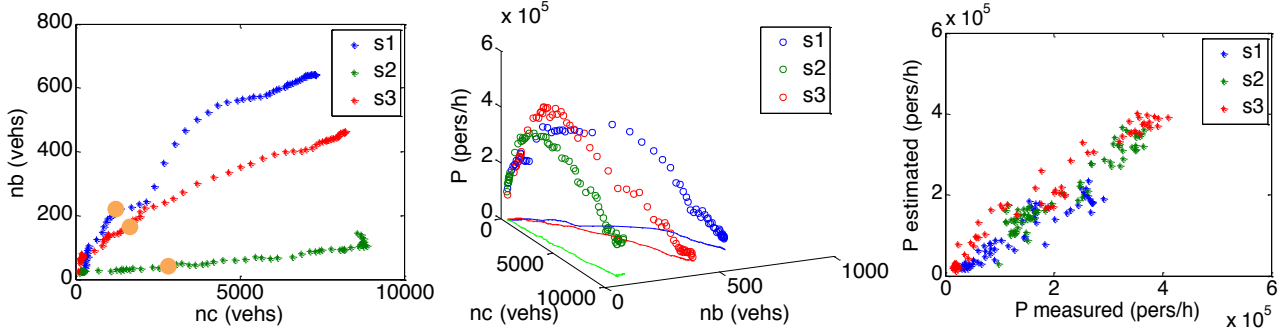
Fig. 10. Comparison of (a) n_c vs. n_b for the entire network; (b) The estimated 3D-pMFD; and (c) The measured P vs. the estimated P by model (13) for the three scenarios.

4   Discussion

In this paper, we extended the single-mode network MFD model to a bi-modal three-dimensional MFD, with the consideration of passenger flows in addition to vehicle flows. We investigated the relation between the accumulation of cars and buses, and circulating flow of vehicles and passengers. We have shown via simulation experiments that: (i) an exponential-family function fits well the data points, (ii) the network's vehicle circulating flow decreases monotonically with the number of buses serving in the network, while the passenger throughput is maximized at a non-zero accumulation of buses. Then, we investigated the derivation of the passenger-flow 3D-MFD with an elegant analytical model. Furthermore, we showed that by applying a partitioning algorithm, which clusters a center and an outside region of the network according to the similarity of the car/bus density ratio, the passenger 3D-MFD model was able to reproduce the observed flow pattern from the simulated data.

The findings of this paper are promising because the concept of a 3D-MFD can be used: (i) to monitor traffic performance in bi-modal networks, and traffic flow dynamics can be predicted given the current state of the two modes, (ii) to develop simple control policies in such a way that maximizes the bi-modal network vehicle or passenger throughput as in Ampountolas et al. (2014) and (iii) to identify different control strategies for different regions of a heterogeneous bi-modal urban network. Furthermore, policy-makers can adjust management measures to operate a city at different mobility levels as expressed by the MFD in Fig. 3(b). An expansion in the bus fleet of a city associated with a congestion pricing scheme to facilitate demand shift from cars to buses can succeed these goals. Further research is needed towards this direction. Ongoing work investigates (i) how perimeter control of cars can improve the system operation and decrease total passenger delays, and (ii) how optimal coordinated control strategies for different regions of a network with different multimodal characteristics can be developed.

Preferential treatment of buses in terms of control strategies should be another research priority. Transit priority strategies for mixed usage lanes and dedicated bus lanes should be carefully investigated. TSP can be more impactful, especially in case of high frequencies of buses. TSP can also influence the shape of the MFD and a methodology to identify critical intersections should be identified to avoid a negative network effect. Typically TSP is activated by the presence of the transit vehicle at certain time periods. Moreover, predicting aggregate behavior of a large number of public transit (PT) lines is easier than predicting the specific behavior/effect of one PT line and TSP. The results of this paper can also facilitate decisions about the redistribution of urban space among different modes as in Zheng and Geroliminis (2013).

Acknowledgement

References

Aboudolas, K. and Geroliminis, N., 2013. Perimeter and boundary control in multi-reservoir heterogeneous networks. Transportation Research Part B 55, pp. 265-281.

Ampountolas, K., Zheng, N. and Geroliminis, N., 2014. Perimeter flow control for bi-modal urban road networks. The 93rd Annual Meeting of Transportation Research Board, Washington D.C., USA, 12-16 Jan 2014.

Boyaci, B. and Geroliminis, N., 2011. Estimation of the network capacity for multimodal urban systems. Procedia - Social and Behaviroal Sceiences 16, pp. 803-813.

Buisson, C. and Ladier, C., 2009. Exploring the impact of homogeneity of traffic measurements on the existence of Macroscopic Fundamental Diagrams. Transportation Research Record 2124, pp. 127-136.

Bureau of Public Roads, 1964. Traffic Assignment Manual. U.S. Department of Commerce, Urban Planning Division, Washington D.C., USA.

Christofa, E., Aboudolas, K. and Skabardonis, A., 2013. Arterial traffic signal optimization: A person-based approach. The 92nd Annual Meeting of the Transportation Research Board, Washington D.C., USA, 13-17 Jan 2013.

Daganzo, C., 2007. Urban gridlock: Macroscopic modeling and mitigation approaches. Transportation Research Part B 41 (1), pp. 49-62.

Daganzo, C., and Cassidy M., 2008. Effects of high occupancy vehicle lanes on freeway congestion. Transportation Research Part B 42 (10), pp. 861-872.

Daganzo, C., and Geroliminis, N., 2008. An analytical approximation for the macroscopic fundamental diagram of urban traffic. Transportation Research Part B 42 (9), pp. 771-781.

Daganzo, C., Gayah, V. and Gonzales, E., 2011. Macroscopic relations of urban traffic variables: bifurcations, multivaluedness and instability. Transportation Research Part B 45 (1), pp. 278-288.

De Berg, M., Cheong, O., van Kreveld, M. and Overmars, M. (eds.), 2008. Delaunay Triangulations. In: Computational Geometry: Algorithms and Applications. 3rd Edition. Springer-Verlag.

Eichler, M. and Daganzo, C., 2006. Bus lanes with intermittent priority: Strategy formulae and an evaluation. Transportation Research Part B 40 (9), pp. 731-744.

Edie, L., 1963. Discussion of traffic stream measurements and definitions. In: Proceedings of the 2nd International Symposium on the Theory of Traffic Flow, Paris, France, 25-27 July 1963, pp. 139-154.

Gayah, V. and Daganzo, C., 2011. Clockwise hysteresis loops in the Macroscopic Fundamental Diagram: An effect of network instability. Transportation Research Part B 45 (4), pp. 643–655.

Geroliminis, N. and Daganzo, C., 2008. Existence of urban-scale macroscopic fundamental diagrams: some experimental findings. Transportation Research Part B 42 (9), pp. 759-770.

Geroliminis, N. and Sun J., 2011. Properties of a well-defined macroscopic fundamental diagram for urban traffic. Transportation Research Part B 45 (3), pp. 605-617.

Geroliminis, N. and Boyaci, B., 2012. The effect of variability of urban systems characteristics in the network capacity. Transportation Research Part B 46 (10), pp.1607–1623.

Godfrey, J., 1969. The mechanism of a road network. Traffic Engineering and Control 11 (7), pp.323-327.

Gonzales, E., Chavis, C., Li, Y. and Daganzo, C., 2011. Multimodal transport in Nairobi, Kenya: Insights and recommendations with a macroscopic evidence-based model. The 90th Annual Meeting of the Transportation Research Board, Washington D.C., USA, 23-27 Jan 2011.

Gonzales, E. and Daganzo, C., 2012. Morning commute with competing modes and distributed demand: User equilibrium, system optimum, and pricing. Transportation Research Part B 46 (10), pp. 1519-1534.

Haddad, J. and Geroliminis, N., 2012. On the stability of traffic perimeter control in two-region urban cities. Transportation Research Part B 46 (9), pp. 1159–1176.

Haddad, J., Ramezani, M., Geroliminis, N., 2013. Cooperative traffic control of a mixed network with two urban regions and a freeway, Transportation Research Part B Methodological, 54, pp. 17-36, 2013.

Ji, Y., Daamen, W., Hoogendoorn, S., Hoogendoorn-Lanser, S. and Qian, X., 2010. Macroscopic fundamental diagram: investigating its shape using simulation data. Transportation Research Record 2161, pp. 42-48.

Ji, Y. and Geroliminis, N., 2012. On the spatial partitioning of urban transportation network. Transportation Research Part B 46 (10), pp. 1639-1656.

Keyvan-Ekbatani, M., Kouvelas, A., Papamichail, I. and Papageorgiou, M., 2012. Exploiting the fundamental diagram of urban network for feedback-based gating. Transportation Research Part B 46 (10), pp. 1393-1403.

Knoop, V., Hoogendoorn, S. and van Lint, H., 2013. The impact of traffic dynamics on the Macroscopic Fundamental Diagram. The 92nd Annual Meeting of the Transportation Research Board, Washington D.C., USA, 13-17 Jan 2013.

Li, J., Song, M. and Zhang, W., 2010. Planning for bus rapid transit in single dedicated bus lane. Transportation Research Record 2111, pp. 76-82.

1   Mahmassani, H., Williams, J. and Herman, R., 1987. Performance of urban traffic networks. In: Proceedings of the 10th International
2   Symposium on Transportation and Traffic Theory, Massachusetts, USA, 8-10 Jul 1987, pp. 1-20.

3   Mahmassani, H., Saberi, M. and Zockaie A., 2013. Urban network gridlock: Theory, characteristics, and dynamics. Transportation
4   Research Part C 36, pp. 480-497.

5   Mazloumian, A., Geroliminis, N. and Helbing D., 2010. The spatial variability of vehicle densities as determinant of urban network
6   capacity. Philosophical Transactions of Royal Society A 368 (1928), pp. 4627-4648.

7   Mesbah, M. and Currie, G., 2011. Optimization of transit priority in the transportation network using a genetic algorithm. IEEE
8   Transactions on Intelligent Transportation Systems 12 (3), pp. 908-919.

9   Saberi, M. and Mahmassani, H., 2012. Exploring properties of network-wide flow-density relations in a freeway network.
10   Transportation Research Record 2315, pp. 153-163.

11   Shi, J. and Malik, J., 2000. Normalized cuts and image segmentation. IEEE Transactions on Pattern Analysis and Machine Intelligence
12   22 (8), pp.888–905.

13   Site, P. and Filippi, F., 1998. Service optimization for bus corridors with short-run strategies and variable vehicle size. Transportation
14   Research Part A 32 (1), pp. 19-38.

15   Tirachini, A. and Hensher, D., 2011. Bus congestion, optimal infrastructure investment and the choice of a fare collection system in
16   dedicated bus corridors. Transportation Research Part B 45 (5), pp. 828-844.

17   Tuerprasert, K. and Aswakul, C., 2010. Multiclass cell transmission model for heterogeneous mobility in general topology of road
18   network. Journal of Intelligent Transport Systems: Technology, Planning, and Operations 14 (2), pp. 68-82.

19   Zheng, N., Waraich, R., Axhausen, K. and Geroliminis, N., 2012. A dynamic cordon pricing scheme combining the Macroscopic
20   Fundamental Diagram and an agent-based traffic model. Transportation Research Part A 46 (8), pp. 1291–1303.

21   Zheng, N. and Geroliminis. N., 2013. On the distribution of urban road space for multimodal congested networks. Transportation
22   Research Part B 57, pp. 326-341.

23   Zheng, N., Aboudolas, K. and Geroliminis, N., 2013. A city-scale macroscopic fundamental diagram for mixed bi-modal urban traffic.
24   In: Proceeding of the 16th IEEE Conference on Intelligent Transportation System, The Hague, The Netherland, Oct 6-9 2013, pp.
25   1029-1034.

26